8257b Journal of Vacuum Science & Technology B
8(1990)Nov./Dec., No.6, New York,US

D1 G11C11/54
G06F15/06C2

E

Electronically wired petri dish: A microfabricated interface to the biological neuronal network

p 1392-1398

M. D. Eggers[a] and D. K. Astolfi
Lincoln Laboratory, Massachusetts Institute of Technology, Lexington, Massachusetts 02173

S. Liu
Brain and Cognitive Science Department, Massachusetts Institute of Technology, Cambridge, Massachusetts 02139

H. E. Zeuli and S. S. Doeleman
Lincoln Laboratory, Massachusetts Institute of Technology, Lexington, Massachusetts 02173

R. McKay
Brain and Cognitive Science Department, Massachusetts Institute of Technology, Cambridge, Massachusetts 02139

T. S. Khuon and D. J. Ehrlich
Lincoln Laboratory, Massachusetts Institute of Technology, Lexington, Massachusetts 02173

(Received 29 May 1990; accepted 3 August 1990)

Presented is the design, fabrication, and evaluation of 72-channel microcircuit electrode arrays (biochips) built to interface neurons and computers. Contributions include a detailed mathematical model of the electrode/electrolyte interface and subsequent electrode design optimization (in terms of maximum signal-to-noise ratio). Electrode impedance measurements were obtained with the electrodes submerged in electrolytic neural solution. Large sample results indicate a 7% discrepancy between theoretical and measured impedances. In addition to the engineering efforts, biological cell culturing techniques were developed to enable the growth of synaptically interconnected, electrically excitable cells on the biochip. Both dissociated invertebrate neurons and clonal mammalian cell systems were employed. Together these contributions enabled microvolt signals to be recorded from *individual* neurons grown and synaptically interconnected on the biochip surface. Also recorded were neuronal responses to on-chip stimulation. Consequently, the biochip technology presented represents a step towards a long-term, noninvasive, multisite electrical stimulation and recording capability necessary for extracting the mechanisms governing the way living neural networks connect, integrate, and self-organize.

I. INTRODUCTION

The current enthusiasm for neural network analogs fabricated in semiconductors is based on scant data on the real operation of biological nervous systems. Brain-probe and similar invasive techniques are of limited practical value in gathering such network data because of the morphological complexity and the fragility of the fully functioning biological organism. Towards extracting a more complete picture of network behavior, various multielectrode microcircuits have been developed for *in vitro* experimentation. Thomas *et al.*[1] are credited for the novel concept of bringing cells to the sensor rather than the sensor to the cells. Although network behavior was observed from the spontaneous rhythmic contractions of heart cells, no electrical recordings from single cells were obtained. Later Gross[2,3] and Pine[4] successfully obtained electrical recordings from neurons clustered on substrates. Inspired by the earlier microcircuit works cited, this paper describes the development of a biologically compatible microcircuit technology aimed at interfacing living neural networks and computers for network experimentation. The concept of the "biochip" is illustrated in Fig. 1. Basically, an array of microelectrodes embedded in a biologically compatible substrate is fabricated using conventional microfabrication techniques. Since the electrodes are embedded in the surface, neurons can grow in contact with the electrodes and their electrical properties monitored as they differentiate. The approach presented differs from those cited above because of the stimulation capability introduced, detailed electrode modeling and optimization, and the reduction of neural network complexity by selectively choosing and placing neurons on the microcircuit, preferably one or more electrodes per neuron.

II. BIOCHIP ENGINEERING

A. Neural signal source

The neuron is a clever information processor that relies on electrical signaling for both short- and long-distance communication. Specifically, the neuron supports long-distance network communication by transmitting high-frequency (1 kHz)/high-voltage (70–110 mV) pulses along the neural output channel (axon). These pulses can be recorded via intracellular (conventional) or extracellular techniques as diagrammed in Fig. 2. The intracellular signal is known as the membrane potential, since the voltage signal is due to the electrical charge imbalance (among Na, K, and Cl ions)

8257b Journal of Vacuum Science & Technology B, 8(1990)Nov./Dec., No.6, New York,US

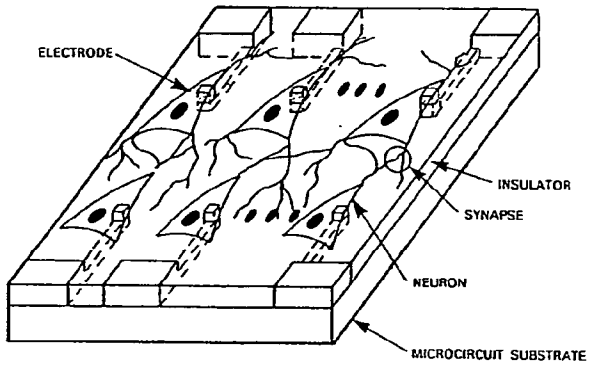

FIG. 1. Illustration of the biochip concept where neurons are grown over an array of microelectrodes used for noninvasive stimulation and recording.

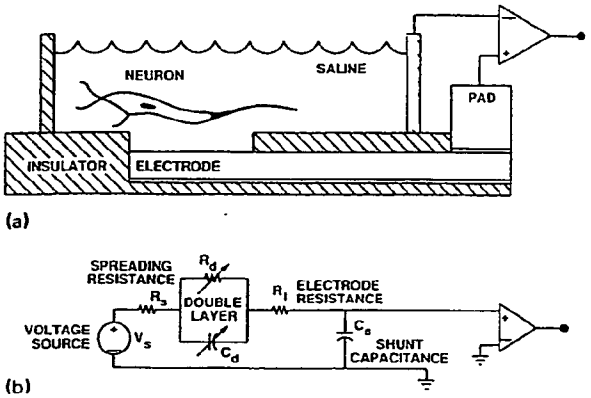

FIG. 3. (a) Diagram of microcircuit electrode exposed to a homogeneous conducting solution for extracellular recording and (b) accompanying reduced equivalent electrical circuit.

across the biological membrane. In fact, the generation of the large membrane potentials for long-distance transmission is due to a change in membrane permeability that effectively alters the distribution of these ions across the membrane. Conversely, the extracellular signal arises from the electrical charge imbalance near the outside of the biological membrane. In contrast to the intracellular potential, this potential is recorded *outside* the neural membrane with respect to the neutral extracellular fluid as diagrammed in Fig. 2. Moreover, the extracellular potential is typically in the microvolt range, while the intracellular potential is measured in millivolts. As a consequence, the three orders of magnitude decrease as signal strength warrants careful electrode modeling and design.

B. Biochip design

The biochip design approach involves first expressing the electrical characteristics of the electrode in terms of the microcircuit dimensions, then subsequently defining a cost function in terms of these electrical characteristics, and finally optimizing the cost function to yield the optimal electrode design. The electrical characteristics of a microelectrode in a homogeneous conducting medium can be modeled as an equivalent electrical circuit, with each electrical component expressed in terms of the fundamental electrode dimensions (see Fig. 3). The general approach follows the

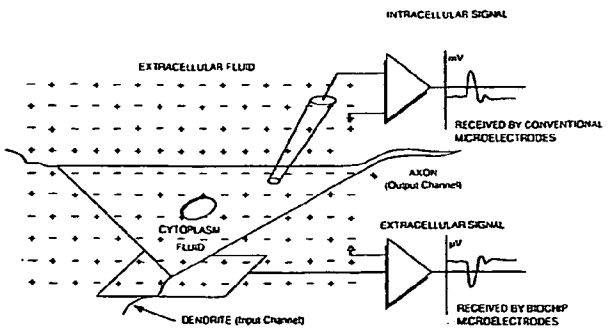

FIG. 2. Typical intracellular (conventional) and extracellular (biochip) neuron recording methods.

treatment of Robinson[5] for conventional glass-coated wire electrodes, however, new techniques are presented where appropriate for the specific microfabrication application.

The neuron, for purposes of an equivalent electrode circuit, is modeled as an ideal voltage source. The voltage V_s is equal to the extracellular voltage that would be recorded immediately outside the axon wall and is referenced to the electrically neutral homogeneous conducting solution. The spreading resistance R_s is the resistance of the homogeneous conducting solution between the metallic electrode and the metal ground ring. The resistance can be derived by integrating the differential resistance along the current path perpendicular to the conducting surfaces to yield[6] $R_s = \rho / (W_c \sqrt{4\pi H / D})$, where H and D are the height and diameter of the ground ring, while W_c is the width of the square electrode contact.

Next, the complex electrochemical reactions at the interface of the metal electrode and electrolyte constitute an electric double layer. The high-impedance electric double layer arises from the trapped separation of charge at the interface (comprised of surface charge on the metal and diffuse counter charge of equal magnitude in the solution). Two methods can be used to obtain the double-layer equivalent circuit components R_d and C_d. The first involves relying on published results for conventional glass-coated bright platinum microelectrodes calibrated in physiological saline solution. Under such circumstances, both R_d and C_d have been found to vary as $\omega^{-1/2}$, while the impedance phase θ_d remains near $-45°$, within the frequency band of interest (100 Hz–10 kHz).[7,8] Imposing these conditions upon the parallel RC model yields the relationship $R_d = 1/\omega C_d$, where C_d is determined from published empirical results [20 μF/cm^2 (Ref. 5)]. An alternative method for obtaining the double-layer circuit components involves conducting an independent calibration experiment utilizing the actual physiological saline solution and electrode metal used for the biochip neural experiments. The calibration experiment described in Ref. 6 enables isolation of the required circuit components R_d and C_d by providing a *macroscopic* environ-

ment where other electrical effects become negligible. Here the microcircuit double-layer component C_d is computed by $C_d = C^0_{d/A} A_e$, where $C^0_{d/A} = C^0_d/2\pi(r^0)^2$ is the capacitance normalized to the calibration *macro*electrode surface area and A_e is the *micro*electrode surface area. In turn, the leakage resistance for the *micro*electrode is computed by $R_d = -\tan\theta^0_d/\omega C_d$, where both C^0_d and θ^0_d are easily derived from the empirical calibration impedance measurements.

The resistance R_l of the metal conductor carrying current from the electrode to the microcircuit bonding pad is comprised of two components. The first resistive component is attributed to the adhesive metal (titanium), while the second is due to the conducting metal (gold). Hence the line resistance for the double-layered conductor becomes

$$R_l = \frac{\rho_1\rho_2}{D_{l_1}\rho_1 + D_{l_1}\rho_2}\frac{L_l}{W_l},$$

where ρ_1 and ρ_2 are the resistivities of the adhesion and conductor layers, respectively, L_l and W_l are the length and width of the electrode line, while D_{l_1} and D_{l_2} represent the depth of the respective layers comprising the electrode line. Finally, the capacitance C_s accounts for the current which is shunted from the electrode line to ground. This shunt capacitance is modeled as a parallel plate capacitor, with the metal electrode line representing the bottom plate and the electrolyte solution representing the upper conducting plate and is given by $C_s = (k\epsilon_0 L_l W_l)/D_i$, where k is the dielectric constant, ϵ_0 is the permittivity, L_l and W_l are the length and width of the electrode line under the electrolyte, respectively, and D_i is the depth of the insulating dielectric. Consequently, using these previously derived formulas for the equivalent microcircuit electrode components, the overall system impedance defined across the electrode pad and ground ring can be obtained.

The system impedance of the microcircuit electrode submerged in a homogeneous conducting medium is given in approximate form ($C_d \gg C_s$) by[6] $Z'' = R_d/\sqrt{1+(\omega R_d C_d)^2}$ with phase $\theta'' = \tan^{-1}(-\omega R_d C_d)$. Another expression follows from assuming similar conditions supporting published results obtained from conventional glass-coated bright platinum microelectrodes calibrated in physiological saline solution. Here C_d and R_d also dominate the system impedance, but in addition the double-layer phase remains constant at $\theta_d \cong -45°$,[5] thus yielding $Z' = R_d/\sqrt{2}$ with phase $\theta' = \tan^{-1}(-\omega R_d C_d) = -45°$.

Optimization of the microcircuit electrode design proceeds by defining a signal-to-noise ratio (SNR) cost function in terms of the previously derived equivalent circuit components. Hence mathematically optimizing this cost function corresponds to selecting the electrode dimensions to ensure the largest received electrode signal given the present noise. The SNR is expressed as $\mathrm{SNR} = P_S/P_N = V_s^2/4kT\Delta_f R_1$, where $k = 1.38\times10^{-23}$ J/K (Boltzmann constant), T is the operating temperature, Δ_f is the signal bandwidth, and $R_1 = R_s + R_l + [R_d/(1+\tan^2\theta_d)]$. Observe that optimizing the SNR design cost function corresponds to minimizing the double-layer resistance term $R_d/(1+\tan^2\theta_d)$, since typically $R_d \gg (R_s + R_l)$ and both the temperature and bandwidth are fixed. In turn, minimization of the double-layer resistance term corresponds to maximizing the electrode surface area A_e, because for the calibration method outlined for obtaining R_d and C_d,

$$\mathrm{SNR}'' = \frac{(1+\tan\theta^0_d)V_s^2\omega C^0{}_{d/A}}{4kT\Delta_f\tan\theta^0_d}A_e.$$

As a consequence, an optimal microcircuit electrode design using *conventional* fabrication techniques simply corresponds to choosing the electrode surface area A_e large as possible. An upper bound for the area is determined by the density of the connecting neurons, for too large an electrode will invite crosstalk from neighboring neurons. Typically the electrode area is designed approximately the size of the neuron to avoid unwanted crosstalk in modest density networks. Hence further increasing the SNR requires increasing the surface area while simultaneously maintaining a fixed electrode footprint of the order of the cell body size. This can be achieved by electrically platinizing the microcircuit electrodes to create a rough porous surface several times greater in surface area. The enhanced effect of platinizing on the SNR can be as much as 20 dB.

Finally, it is important to realize that although mathematically optimal electrodes can be designed as discussed, the actual behavior of the electrode surrounded by neural tissue will vary from prediction. The deviation is attributed to the complex pattern of ionic currents that develop surrounding each of the current generating neurons. Consequently, the modeling and subsequent design optimization based on a homogeneous conducting medium (isotonic saline solution) offers much towards providing insight and general design guidelines, but should not be mistaken as an accurate representation of experimental conditions surrounding nonhomogeneous neural networks.

C. Biochip fabrication

Primarily conventional microfabrication substrates and techniques can be employed to fabricate the previously designed biochip electrode arrays. Successful neural growth has been achieved on glass, silicon, and silicon dioxide (quartz). Quartz is favorable because the clear substrate enables viewing during neural experimentation using a transmission microscope, and is dimensionally stable at the high temperatures required for processing. Regarding fabrication, the electrode pattern is made by first treating the chosen substrate with an adhesion promoter. A solution of 50% hexamethydlisilazane (hmds) and 50% xylene is puddled on and allowed to sit for about 10 s. The substrate is then spun at 3000 rpm to remove all but a monolayer of hmds. One-half micrometer of positive photoresist (Shipley S1805) is then spun onto the wafer and baked for 30 min at 90 °C in flowing air. Next, the substrate is placed in vacuum contact with a 60-mil-thick glass mask bearing the electrode pattern in an ultraviolet (UV) opaque material. The photoresist is exposed to UV light through this mask. Subsequently, the substrate is dipped in developer to remove the photoresist which has been exposed to the light. This leaves

8257b Journal of Vacuum Science & Technology B
8(1990)Nov./Dec., No.6, New York,US

photoresist everywhere except on the electrode pattern. Using an electron-beam evaporator, 10 nm of titanium is then deposited onto the substrate followed by 50 nm of gold. The photoresist is removed in acetone "lifting off" the metal that has been deposited on the surface, hence leaving only the electrode pattern in gold. Next the dielectric insulation layer is deposited. Depending on the design, 2000–4000 Å of silicon dioxide (SiO_2) is deposited using chemical vapor deposition. After covering the entire surface with SiO_2, holes must be cut to expose the ends of the electrodes. The substrate is coated with one-half micrometer of photoresist and baked as before. Using a contact aligner, the photoresist is exposed with the hole pattern aligned to the electrode pattern. After developing, using the photoresist as a mask, the SiO_2 is etched through in a plasma etcher using a mixture of CF_4 and O_2. The photoresist is then removed in ACT-1 resist stripper at 90 °C. Finally, the microcircuit is ready for packaging into a 72-lead gold-plated package, with a hole cut in the back for microscopic viewing. After being epoxied into the package, the package leads are wire bonded to the bonding pads using gold wire. A gold-coated ring is then epoxied to the center of the circuit to isolate the growth solution, and act as the ground connection for the electrical measurements. A picture of the 72 unipolar electrode array is shown in Fig. 4 with 5-μm lines and 10-μm-square electrodes.

Evaluation results from the best fabrication run (565 electrodes were operable among 8 biochips) are shown in Fig. 5. Notice the exact impedance function[6] and the approximation function that incorporates the calibration yield approximately (2%) the same values, while the other approximation method based on published capacitance values is

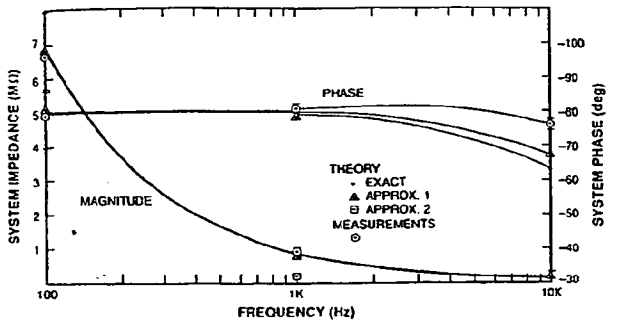

FIG. 5. Graph of theoretical and measured biochip electrode impedances. The theoretical curves are from the complete impedance expression (Ref. 6), and approximate forms given by Z^* and Z'. The measurements are taken across an electrode bonding pad and the conducting ground ring (shown in Fig. 3).

significantly different (74%). The discrepancy is attributed in part to the specific neural growth solution used and the gold electrode metal. Both are different from those substances used in the published calibration experiment from which $C_{d/A}$ was obtained.[5] Comparing the measured values to the exact and first approximation theoretical results, good conformance is displayed especially at 1 kHz where less than 7% difference is reported. Consequently, the evaluation results substantiate the particular electrode modeling approach introduced based on the calibration experiment from which the electrical double-layer components were obtained. Also the use of the first approximation impedance function appears warranted.

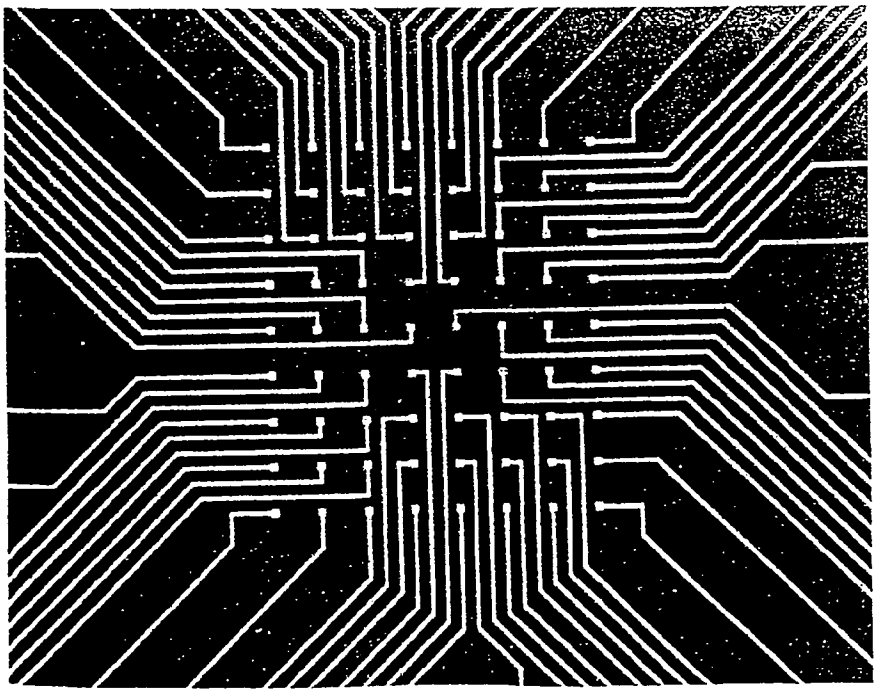

FIG. 4. Biochip with 5-μm lines and an array of 72 10-μm-square unipolar electrodes.

8257b Journal of Vacuum Science & Technology B
8(1990)Nov./Dec., No.6, New York,US

D. System integration

The integration of the neural network signal processing system, ranging from the biochip (with microvolt analog signals) to the computer (with digital signals), consists of building custom instrumentation amplifiers and neuronal chambers to house the biochip. The specifications for the instrumentation amplifier are driven by the neural signaling properties, together with biological considerations. Regarding neural signaling, the extracellular action potentials may range from 50 to 400 μV peak-to-peak and are embedded in 20–40 μV thermal noise, while the bandwidth is generously selected at 7 kHz. Therefore, the amplification required is approximately 50 000. Considering the biology, the neuron must be isolated from the electronics to avoid induced behavior artifacts. Hence a very large amplifier input impedance is required. Moreover, a low bias current is necessary so that the high gain amplifier will not saturate when connected to the high-impedance (MΩ) electrode source. A two-stage custom amplifier satisfying these constraints utilizes a Burr-Brown INA110 very-high-accuracy instrumentation amplifier and a subsequent conventional operational amplifier (AD711BQ) for additional gain. The front-end amplifier offers the desired high input impedance (1 TΩ) by using dual-precision FET buffers on the input. This design also affords a low dc bias current (50 pA) to avoid saturation, and low input current noise (1.8 fA/$\sqrt{\text{Hz}}$). Finally, the variable gain is set to 500 such that in combination with the second stage, the overall gain is near 50 000. The frequency response of the amplifier is shaped to provide a 3 dB bandpass extending from approximately 170 Hz to 8 kHz. Finally, regarding neuronal chambers, the specific chamber employed for the mammalian cells is displayed in Fig. 6. The metallic walls house a heating coil which is thermostatically controlled. Also the innermost sterilized chamber fits over the biochip package for easy assembly. The neuronal chamber designed for the invertebrate cells is shown in Fig. 7. Here a standard flatpack socket with matching carrier suffices since temperature need not be controlled.

III. NEURAL MEASUREMENTS

This section demonstrates the neural recording and stimulation capabilities of the biochip. Two measurement experiments are described that demonstrate the ability to record from both single neurons, and a network of neurons grown and synaptically coupled on the biochip. The objective of the single-neuron recording experiment is to verify the basic technology development and recording operation of the biochip. Here a conventional glass-coated intracellular microelectrode serves as the benchmark recording measurement. The procedure begins by placing dissociated Aplysia neurons on the biochip surface. An intracellular probe is then inserted into a candidate neuron residing over an electrode as shown in Fig. 8. The neuron is subsequently stimulated by the intracellular probe with a current pulse which serves to depolarize the neuron. Recorded neuron signals from both the intracellular probe and the extracellular biochip electrode are also shown. Notice both the intracellular and extracellular recordings display three action potentials with

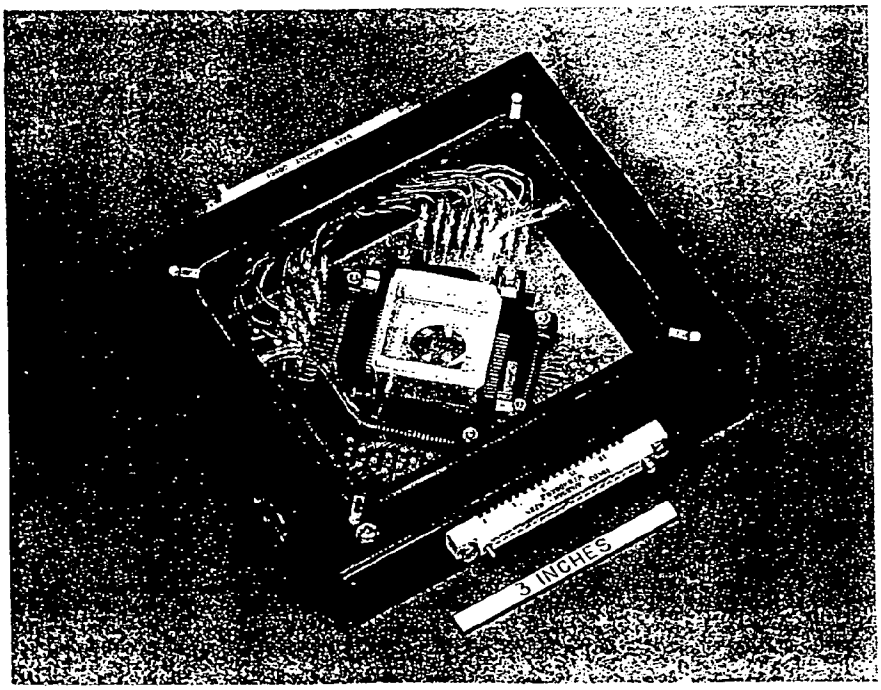

FIG. 6. Neuronal chamber for mammalian cells equipped with temperature and gas control.

8257b Journal of Vacuum Science & Technology B
8(1990)Nov./Dec., No.6, New York,US

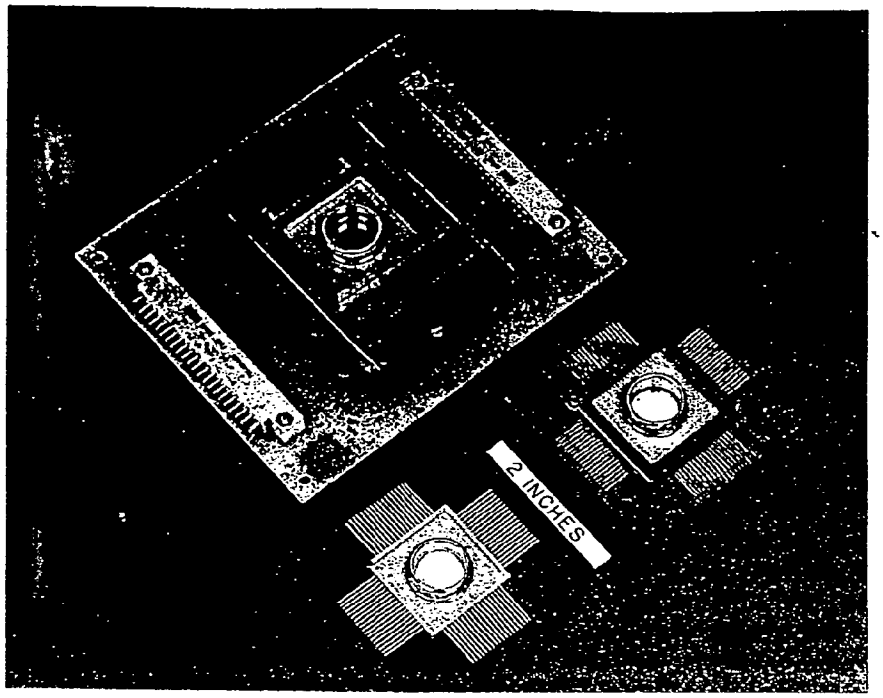

FIG. 7. Neuronal chamber for invertebrate cells employing standard socket and carrier packs.

good correlation. Clearly the price for noninvasive recording is lower SNR, however, the SNR is sufficient to easily discern the microvolt-level extracellular neural response.

The second recording experiment serves to demonstrate that a network of neurons can be grown on the biochip. Again the experiment begins by growing Aplysia neurons on the biochip. Within days the neural processes grow to make connections with neighboring neurons. At approximately 3 days the network displays abundant convoluted connections as shown by the electron micrograph in Fig. 9. Results from a spontaneously active network are shown in Fig. 10. Here no external stimulus is applied, rather, an active rhythmic neuron is selected as the presynaptic neuron, while a connecting neuron is intracellularly probed to obtain the accompanying postsynaptic neural response. Notice the postsynaptic neuron responds to each presynaptic neural input with a correlated graded potential. On occasion, the graded potential is strong enough to elicit an action potential as displayed. Strong correlation in presynaptic and postsynaptic neural signals confirm synaptic connection.

To demonstrate on-chip stimulation capability with the unipolar electrodes, Aplysia neurons are placed on the biochip surface as described earlier. Next a candidate neuron residing over an electrode on the biochip is selected for stim-

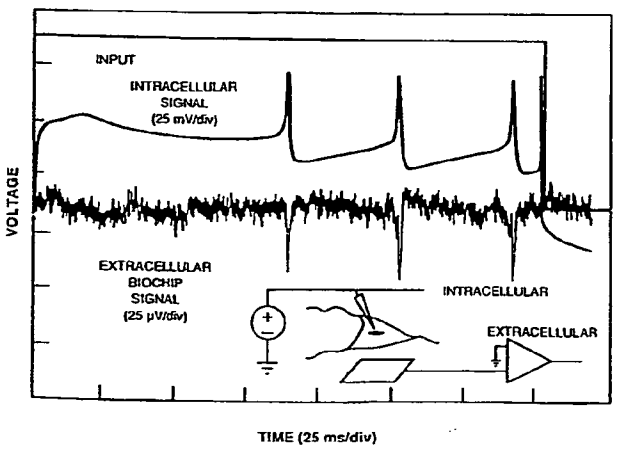

FIG. 8. Single neuron recordings from conventional intracellular and biochip extracellular electrodes. Also shown is the input stimulus pulse.

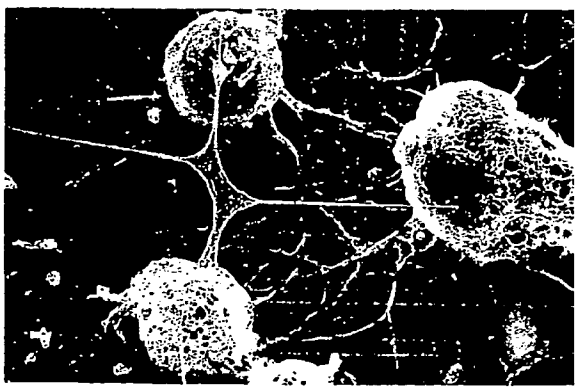

FIG. 9. Electron micrograph of synaptically connected neurons on the biochip surface.

8257b Journal of Vacuum Science & Technology B
8(1990)Nov./Dec., No.6, New York,US

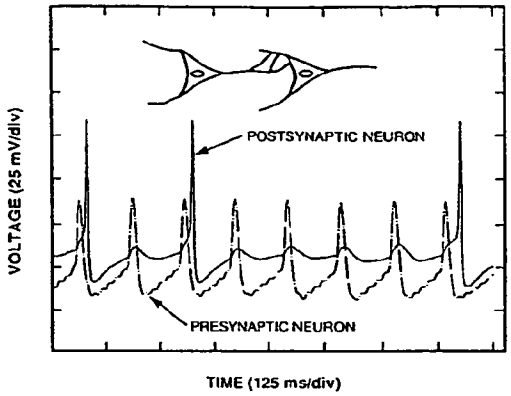

FIG. 10. Recorded intracellular signals from spontaneously active, synaptically coupled neurons on the biochip surface.

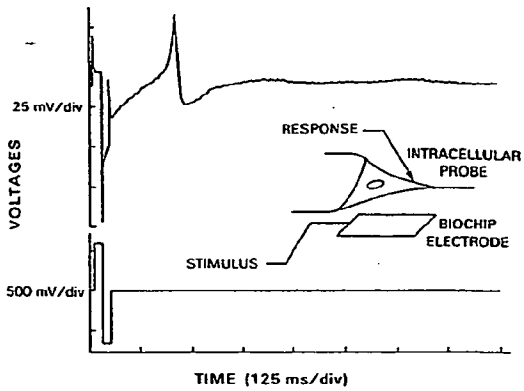

FIG. 11. On-chip neuron stimulation results utilizing a unipolar biochip electrode.

ulation. A conventional intracellular electrode is then inserted for recording purposes, specifically to verify that the on-chip stimulus signal promotes an action potential. The biochip unipolar extracellular electrode is subsequently driven by a symmetric voltage signal source as displayed in Fig. 11. Also shown in the resulting intracellular recording that illustrates the successful depolarization of the neuron leading to the action potential.

IV. CONCLUSIONS

The biochip technology presented provides a foundation for effectively interfacing living cells and electronics. The potential for long-term noninvasive multisite recording and stimulation has been demonstrated. The continued multidisciplinary (electrical engineering, biology, physics) building of such interface is envisioned to be instrumental in both future information technology and medicine. For biologically inspired computer architectures that exploit the principles of superior biological information processing may become reality. In addition, the interface supports medical prosthetic devices for restoration of nerve function.

ACKNOWLEDGMENTS

This work was supported by the Department of the Air Force under Contract No. F19628-85-C-002 and the Pew Foundation. R. M. is a scholar of the Rita Allen Foundation.

[a)] Presently with the Houston Advanced Research Center/Rice University, The Woodlands, Texas, 77381.

[1] C. Thomas, P. Springer, G. Loeb, Y. Berwald-Netter, and L. Okum, Exp. Cell Res. 74, 61 (1972).
[2] G. Gross, IEEE Trans. Biomed. Eng. BME-26, 273 (1979).
[3] M. Droge, G. Gross, M. Hightower, and L. Czisny, J. Neurosci. 6, 1583 (1986).
[4] J. Pine, J. Neurosci. Methods 2, 19 (1980).
[5] D. A. Robinson, Proc. IEEE 56, 1065 (1968).
[6] M. D. Eggers, R. D. McKay, D. J. Ehrlich, D. K. Astolfi, S. Liu, H. E. Zeuli, S. S. Doelman, T. S. Khuon, D. L. Hovey, Y. B. Grinbush, C. Reddies, R. Y. Levine, and S. G. Cann, Biochip Technology Development, TR901, MIT Lincoln Laboratory, 1990.
[7] R. Gesteland, B. Howland, J. Lettvin, and W. Pitts, Proc. IRE 47, 1856 (1959).
[8] H. Schwan, in *Physical Techniques in Biological Research*, edited by W. L. Nastuk (Academic, New York, 1962), Vol. 6, Chap. 6.